Master of Science Thesis

Development of a phantom for optimisation and quality control in functional MRI (fMRI)

Anders Nilsson

Supervisor: Johan Olsrud, PhD

Medical Radiation Physics
Clinical Sciences, Lund
Lund University, 2006

Abstract

BOLD imaging is a useful and promising examination tool for mapping human brain functions, using the local alteration of blood oxygenation in the brain caused by neural activity. However, due to the weak signal response, optimisation of the entire methodology is important in BOLD imaging. To enable optimisation of various examination parameters, a fixed BOLD signal is often desirable. The phantom presented in this work is constructed of two agarose gel types with different T_2 relaxation times, designed to simulate a BOLD response. The phantom has been tested in terms of reproducibility and stability, and additionally to optimise a signal parameter, in this work the echo time. The results show that the phantom can simulate a fixed-amplitude BOLD response used for optimisation of different parameters, such as the echo time. Additionally, the phantom is suitable for stability tests over longer times.

Contents

1. Introduction

1.1. The purpose of this work

This work is focused on construction and evaluation of a phantom and data analysis software, which should be suitable for quality assurance and optimisation of signal detection in clinical BOLD (Blood Oxygen Level Dependent) functional imaging. The phantom and software should offer a way to test signal stability over longer times. It should also offer a way to simulate a block-type BOLD experiment in order to possibly study the influence of various parameters such as coil types, pulse sequences and imaging parameters on BOLD sensitivity.

Specifically, the work is conducted as follows:

- General requirements on a phantom that should simulate the BOLD effect are given and a phantom consisting of two gel compartments is designed.
- The phantom is manufactured and the relaxation properties (T_1 and T_2) of the gel compartments are confirmed.
- A computer program to be used for the data analysis is constructed.
- To evaluate the phantom in practice, it is used to measure scanner stability and to perform BOLD measurements resulting in t-maps similar to those in an fMRI experiment.

The BOLD measurements are done A) to assess the reproducibility between scan sessions and B) to verify the optimum echo time with respect to CNR (TE=T_2*), where T_2* is known for the phantom.

1.2. History and basic principles of fMRI

Blood oxygen level dependent functional magnetic resonance imaging (denoted BOLD fMRI) is a relatively new tool in neuroradiology, in which changes of blood oxygenation in the brain can be detected and related to brain function. The method is based on the discovery that a local increase in neuronal activity gives rise to a change in local blood flow, local blood volume, metabolism, oxygen utilization and subsequently in blood oxygenation (Ogawa *et al.* 1990, Kwong *et al.* 1992, Noll 2004).

The first experiments with functional MRI were performed in the early 1990s and used gadolinium contrast to detect increases in blood volume during a stimulus (Belliveau *et al.* 1991*)*. The use of contrast agents soon became obsolete after the discovery that the changes in blood flow could itself be used as a contrast agent (Ogawa *et al.* 1990, Ogawa *et al.* 1990b). Oxygenated blood (oxyhemoglobin) is diamagnetic, but when oxyhemoglobin loses its oxygen, the resulting deoxyhemoglobin becomes paramagnetic. As the human tissue is less paramagnetic compared to deoxygenated blood, this results in a difference in magnetic susceptibility between the deoxygenated blood and the surrounding tissue. Due to the subsequent susceptibility change, the nuclear spins dephase faster in terms of T_2* relaxation time, causing the signal to decay faster. This gives rise to a signal change relative to the surrounding tissue and an increase in image

contrast (Ogawa *et al.* 1990). With this argumentation, the signal arising from the blood vessels within the activated area would decrease during activation due to the increased oxygen demand; instead a signal increase is observed. The signal increase can be explained due to the fact that during an activation, the oxygen consumption is only slightly increased in the activated area, while the cerebral blood flow (CBF) and the cerebral blood volume (CBV) is increased much more (Fox *et al.* 1988). Regarding the CBF and the CBV, the increase in CBF is approximately 2 - 4 times larger than the CBV increase (Kwong *et al.* 1992). These factors contribute to decrease the local deoxyhemoglobin concentration, which in turn increases the signal.

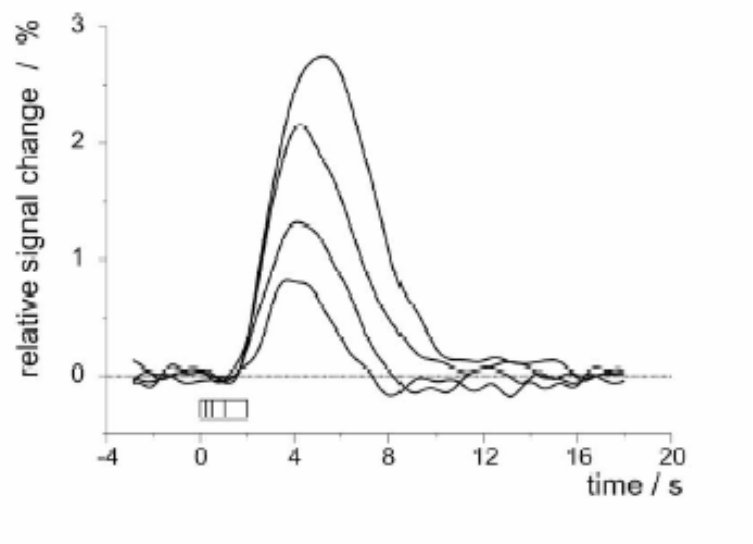

Figure 1. BOLD signal responses to a visual stimuli with different stimuli duration times (250,500,1000 and 2000 ms). Longer stimuli duration times results in lower amplitude and duration of the signal response (redrawn from Pfeuffer et al 2003).

After a given stimuli, the increase in CBV and CBF is slightly delayed relative to the increase in neural response. The result is a delayed temporal signal response between activation and a change in BOLD signal, typically as long as 3 – 6 seconds (Voets *et al.* 2005). After this delay the increase in CBF and CBV makes the signal stronger, see figure 1.

1.3. Clinical BOLD fMRI

The use of BOLD fMRI has increased swiftly, due to several advantages compared to other methods; for example, it is a repeatable examination with no ionizing radiation, which makes it possible to follow different disease and recovery stages over longer times, and it is non-invasive (Gore, 2003). Among the weaknesses are the relatively small signal differences obtained, and the sensitivity to head movement during examination (Lorberbaum *et al.*).

Today a majority of clinical BOLD fMRI examinations are made in presurgical purpose. These examinations makes it possible to find areas corresponding to specific brain functions in the vicinity of resection areas, giving valuable information for planning the resection (Van Westen *et*

al. 2005). The use of BOLD imaging also provides the possibility to examine brain recoveries after injuries such as stroke and surgical resection (Voets and Matthews 2005).

Clinical BOLD imaging is often conducted as a block-test, where the patient is exposed to a stimulus for a fixed time, after which the patient is allowed to rest. This activation/rest combination is repeated several times to get satisfactory statistics, see figure 2. Theoretically, the use of one long activation period followed by one rest period would be possible, but this pattern correlates much easier with signal changes caused by other factors, such as movement or scanner drift. This would result in more false activation and therefore, block-design is more appropriate.

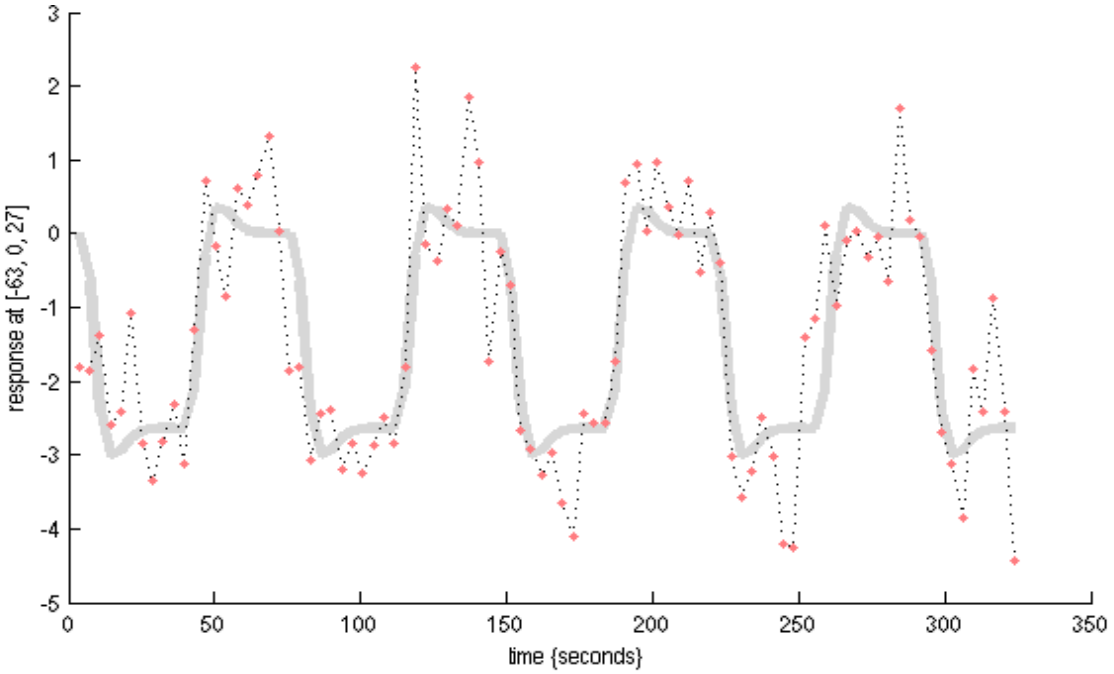

Figure 2. A single-voxel response in the Broca area from a block-type language experiment. Grey line shows a fitted General Linear Model. (By courtesy of Tony Waites, Lund University).

During these intervals of stimuli and rest, images are taken with fast image sequences such as single-shot gradient echo-planar imaging (GRE-EPI). The advantages of gradient EPI sequences are the sensitivity to the BOLD effect, and the speed; images can be taken with intervals less than 100 milliseconds (Lorberbaum *et al.*). However, due to low bandwidth in the phase-encoding direction of the EPI sequence, susceptibility effects also cause spatial distortion and signal void in the images, especially in regions lying close to air (McRobbie *et al*).

The BOLD examination is very sensitive to head movements (Lorberbaum 2005, Voets *et al.* 2005). Investigations have showed that a two degree head rotation can cause changes in T_2^* similar to the BOLD response (Caparelli *et al.* 2004).

The images from the BOLD series are most often statistically compared with a theoretical response, which is constructed by a convolution of the stimulus profile with a hemodynamic response function (HRF), see figure 2.

Because of clinical BOLD images often are acquired at an interval of a few seconds shorter than the T_1 relaxation time, the T_1 relaxation has normally not relaxated fully between the image acquisitions. This results in a shorter magnetisation vector to be affected in the subsequent RF pulse. Thus, the signal becomes weaker compared to the preceding image. This reduction of the vector amplitude continues until a steady-state has been reached, when the M_0-vector length has become stable. To avoid this so called T_1-effect, a number of extra image acquisitions, often called ”dummy-scans”, are added in the very beginning of the BOLD examination, which allows the magnetisation vector to reach a steady-state before the BOLD sequence commences. These dummy scans, often 2 - 3 images, are excluded from the BOLD data.

After exclusion of the initial “dummy-scans”, the remaining images can be considered as members of two groups,”active” and ”rest”. These two groups can be compared in each voxel using a statistical t-test which results in a statistical parameter map (SPM), see figure 3 below.

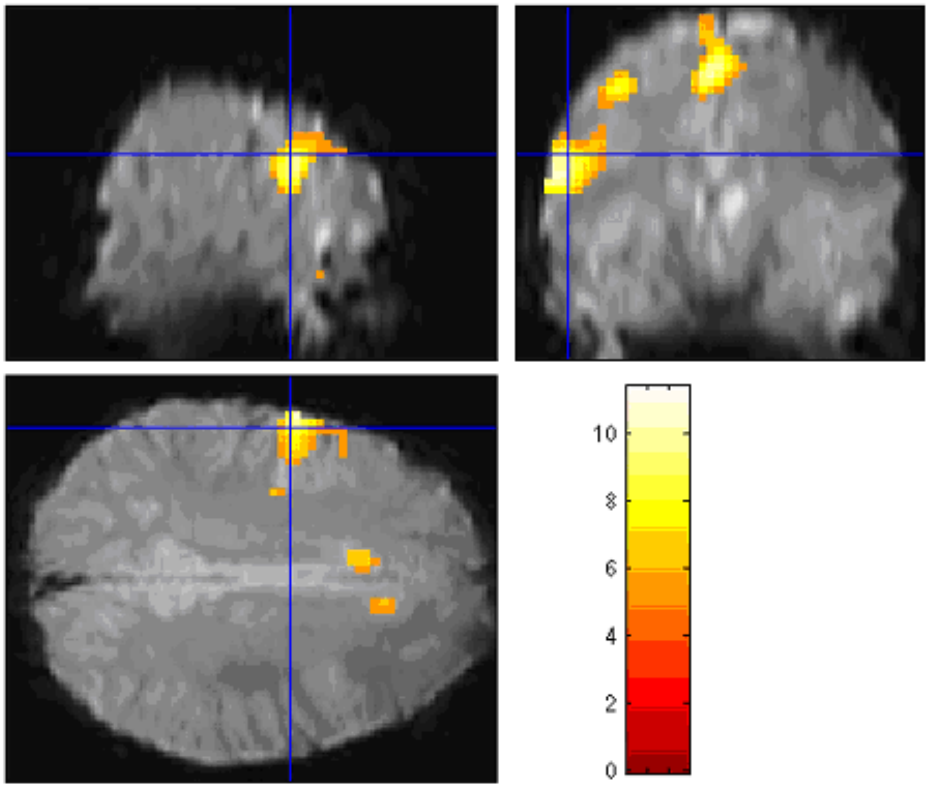

Figure 3. Resulting SPM-chart from a language experiment of an adult man, showing activation in the middle frontal gyrus, which is implicated in language- and working memory function. T-value threshold of 5.15 (By courtesy of Tony Waites, Lund University).

1.4. Could a phantom simulate the BOLD effect?

In BOLD fMRI, the low contrast between activation and rest state puts high demands on the equipment and the design of the examination. For example, the patient must cooperate fully, the MR system must be high-performing (e.g. be sensitive to the BOLD effect and stable over time), the paradigm and timing of the image acquisition needs to be carefully planned, and the postprocessing and statistical assessment needs to be optimised. To optimise several of these steps it would be valuable to have the possibility to obtain a well known and reproducible activation. One way to do this is to add a known artificial activation to fMRI data acquired during a resting state (Olsrud *et al.* 2005). However, this will not fully account for the characteristics of the MR system and the noise is hard to model. A simple and effective alternative would be to use a test object that can produce a specified signal change in the MR images that mimics the BOLD effect. At least one such phantom has recently been presented (Cheng *et al.* 2004).

In general, when designing a test object one needs to consider the effect that is to be simulated, but also any simplifications that can be made based on the desired use of the test object. A BOLD response *in vivo* results in a local magnetic field inhomogenity change in the grey brain matter (GBM), causing the T_2*-relaxation time to temporally increase after a stimuli. To simulate the response, creating a change of the transverse magnetisation, for example by altering the T_2*-relaxation, is necessary. However, the complete imitation of the BOLD effect, including the hemodynamical response, may not be necessary to simulate to optimise the BOLD sensitivity or to perform periodic quality assurance. In this work a phantom with only two relaxation states (activated and rest state) is proposed, which roughly simulates a block-paradigm. This results in easier interpretation and evaluation of the phantom data, although factors such as physiological noise and patient respiratory effects can not be included.
Having done this simplification, we now consider how to alter T_2*. We notice that the T_2* relaxation time depends both on the T_2 relaxation time, and the effect of magnetic field inhomogenities. The T_2 relaxation time describes the dephasing of the spins, and is roughly independent of the field strength. The susceptibility effects caused by field inhomogenities tend to increase in absolute terms with higher field strength, resulting in larger signal differences between activated and rest state with increasing magnetic field strength.

One of the test objects that have been described simulates the BOLD effect with help of additional coils which enhances the radiofrequency (B_1) field (Friedman *et al.* 2005). One alternative approach would be to alter the T_2 relaxation time instead of altering the magnetic inhomogenity. The altering of the T_2 relaxation time can be done by using substances with different T_2 relaxation times. However, to achieve reproducible changes of the T_2* relaxation time, no or small changes of the inhomogenity effects can be allowed. The phantom proposed in this work consists of two agarose gel compartments with different agarose concentrations and thus different but well defined T_2 relaxation times. Making this simplification one needs to evaluate if a well defined change of T_2* can also be obtained.

Normally, the human brain geometry inside the camera during examination does not change, unless the patient is moving. If the geometry would change between two image acquisitions, e.g if the patient would move between two image acquisitions, the following imaging slice would consist of different atoms with respect to the atoms in the preceding image.

The T_1 effect mentioned in section 1.3 applies to a non-moving object. If the object inside the camera would move between image acquisitions, like this phantom, the atoms in the slice plane from the preceding image acquisition would not be identical to those in the slice plane of the following acquisition, and thus the magnetisation vector of the atoms in the first image slice would not reach a steady-state amplitude. For example, if the object is in different positions during activated and rest-state respectively, the T_1-effect would appear in the beginning of each block, resulting in an initial signal raise in the initial images in each block. To avoid such an effect, the first images in each block should be excluded from the dataset, if the object is moved between the blocks.

A common BOLD-examination often yields signal changes equal to 1 – 5 % in the activated areas, where the PSC increases with higher B_0-field strengths (Parrish *et al.* 2000). This range of signal change is assumed to be desirable with the phantom.

When using two different gels with similar T_1 relaxation time, but with slightly different T_2 relaxation times, representing activated and non-activated state respectively, a BOLD response should be possible to imitate by altering which substance is in the slice-plane during the examination. This simple approach is evaluated in this work.

2. Material and Methods

2.1. The phantom design

The principal demand on the phantom is that the T_2*-relaxation time in the slice of interest can be altered in a controlled manner, with respect to both time and position. Another demand is that the change in T_2* should be fairly equal to that of *in vivo* experiments.

These demands have lead to the idea to use two gel substances, with different T_2*-relaxation times, but with equal T_1-relaxation times to simulate the BOLD response. A common way to create gels with known relaxation times and good long-term stability is to use agarose and $NiSO_4 \cdot 6H_20$ solved in distilled water (Christoffersson *et al.* 1991). The two substances affect both T_1- and T_2 relaxation times, although agarose primarily affects T_2 relaxation and Ni primary affects T_1 relaxation.

In the present phantom two gel compartments were used as shown in figure 4. Two gel types are present in the inner cylinder; one which represents the baseline state and one which represents the activated state. To simulate a response and thereby alter the T_2*-relaxation time using this design, a replacement of the gel type needs to be done in the slice plane. During imaging, this replacement introduces a problem with the geometry; a modern camera usually creates a map of the magnetic field inside the camera before examination, which is used to partially correct the influence on the magnetic field homogeneities resulting from susceptibility effects in the object (active shimming). This correction might be hampered if the geometry of the phantom alters significantly during examination. This needs to be considered when designing the phantom. To minimise the effect, the possible influence of an altered geometry on magnetic field homogeneity, the movement of the inner cylinder needed to replace the gel type in the slice plane has to be as small as possible. Additionally, the moving part of the phantom needs to be as homogeneous as possible. Materials other than the gels can produce significant effects if these are to be moved

during imaging. For example, if the two gels in the inner cylinder were to be separated in two chambers by a plastic wall, this could cause severe inhomogeneity effects, for which the shim map would not fully correct for. If the inner cylinder would be moved during examination, this inhomogeneity would be displaced and hence effect the result.

If a wall separating the gel types is not used, that is if the two gel types are in direct contact with each other, the inhomogeneity effects caused by movement are minimised. If using only one slice, this movement can be just a few centimetres, thereby reducing possible effects on T_2^* due to an altered magnetic field homogeneity. (Effects of a separating wall were observed using a previous version of this phantom in this work).

The final design of the phantom consists of an inner cylinder with two gel compartments and an outer cylinder, also filled with gel (figure 5 and 6).

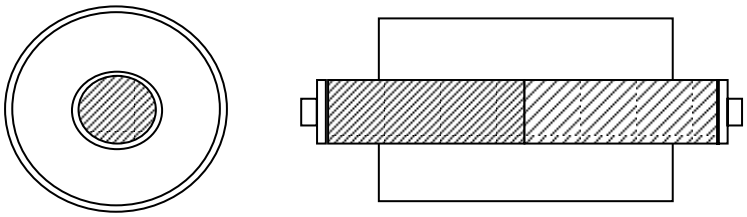

Figure 4. A transverse and sagittal schematic view of the phantom.

The inner cylinder diameter is approximately 50 mm and the cylinder length is equal to 200 mm. The inner cylinder with the two types of gel runs through the outer cylinder, with a diameter equal to 150 mm. The outer cylinder is filled with gel which represents grey brain matter in a non-activated state, similar to the gel in the inner cylinder representing non-activated grey brain matter. The outer cylinder represents the surrounding brain matter and results in a fairly realistic geometry compared to the human head. It also acts as a fixation of the phantom due to its weight, reducing unwanted motion of the phantom in the transversal plane during the movements of the inner cylinder.

The inner cylinder has lids with rubber gaskets in both ends. The outer cylinder is permanently sealed in one end, whereas the other end has a lid with a rubber gasket.

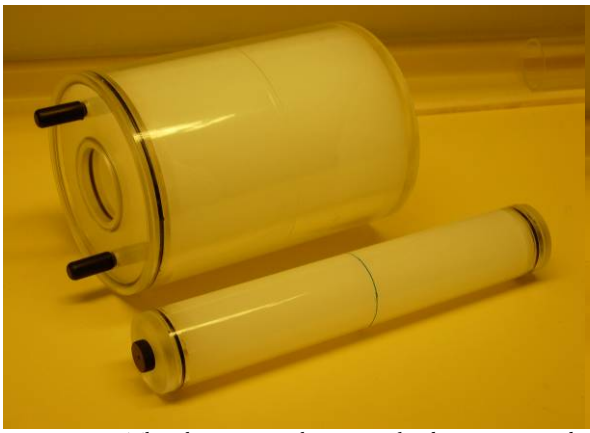

Figure 5. The phantom with inner cylinder unmounted.

Figure 6. The phantom in exam-mode.

2.2. Manufacturing the phantom

To find suitable amounts of Ni and agarose to obtain satisfying values of T_1 and T_2, an Excel worksheet was used, allowing interpolation between experimentally determined relaxation times, resulting from different concentrations of nickel and agarose (Christoffersson 1991, Jonas Svensson, 2004-02-05).

The T_2 relaxation times of the two gels in the inner cylinder were designed to be 50 ms (baseline state) and 55 ms (activated state), respectively. The T_2* relaxation time of the baseline gel were aimed to be approximately equal to the T_2* relaxation time of grey brain matter at a field strength of 3 T. The T_2 in gray brain matter is approximately equal to 80-90 ms (Lu et al 2005), and the corresponding T_2* is significally lower, i.e. approximately 40 - 50 ms (Krüger et al 2001). To create a gel representing baseline state with a T_2* in this range, it was found that the T_2 relaxation time of the gel should approximately be equal to 50 ms.

The T_2 relaxation time for the activated gel was found by using the Bloch equations to find a signal difference between the two gel types of approximately 5 percent. The difference in the T_2 relaxation time was calculated to be approximately 5 ms to get a signal difference equal to 5 percent, at an echo time of 30 ms. The echo time of 30 ms is at present used in clinical BOLD imaging at the Lund University Hospital, and hence this echo time was used in the calculations. Thus, the T_2 relaxation times were aimed to be 50 ms in the baseline gel, and 55 ms in the activated gel.

Both gels were aimed to have identical T_1 relaxation times, close to the T_1 value of grey brain matter. As grey brain matter are reported to have T_1 values in the range of 1000 – 1300 ms at 3 T (Lu et al 2005), a value of approximately 1250 ms were chosen for both gels.

The agarose and Ni concentrations needed for these desirable gel relaxation times were calculated to be 2.44 % agarose together with 0.655 mM Ni for the baseline gel (T_2=50 ms, T_1=1250 ms), and 2.21 % agarose together with 0.682 mM Ni for the activated gel (T_2=55 ms, T_1=1250 ms), respectively. The gel in the outer cylinder was manufactured similarly to the one in the inner cylinder representing baseline state.

Distilled water was poured in a beaker and appropriate amounts of agarose and $NiSO_4$ x $6H_2O$ were added. The mixture was weighted and the beaker top was covered with plastic film after weighting to prevent excessive boil-off during the heating. Next, the beaker was placed in a microwave owen and heated until boiling began. During the heating the mixture was taken out 1 – 2 times and stirred to get a homogeneous mixture. The boiling was allowed to continue for about 30 seconds, where after the beaker was taken out and the plastic film removed. The beaker was weighted and distilled water was added to compensate the amount of water lost during the boiling process. Finally, the mixture was poured into the phantom and was allowed to cool down. Care was taken during the pouring to minimise bubbles in the gel. This procedure was repeated several times, first the gel representing activated GBM was made and poured into the inner cylinder and was allowed to become fixed, where after the next gel representing the non-activated state was made and also poured on top of the first gel. No sign of mixing between the different gels was seen, although it would have been possible that the warm gel would have melted the top layer of the first gel. To prevent this, the second gel was allowed to chill as much as possible without becoming solid before it was poured into the inner cylinder.

The gel dedicated for the outer cylinder was first mixed in one big beaker due to the large volume, where after smaller portions of the solution were heated and poured into the outer cylinder in a rapid sequence. After all the portions had been added to the outer cylinder the solution was carefully stirred.
When the gels had been cooled off, molten paraffin was poured over the gel surfaces to prevent the gel from drying.

2.3. Evaluation of phantom properties

Before using the phantom, the T_1- , T_2 - and T_2*-relaxation times for the manufactured gels were experimentally evaluated, to be certain that they did not differ too much in comparison to the ones aimed at during the manufacturing procedure.

All scans regarding the evaluation of the relaxation properties were made on the Siemens Magnetom Allegra 3T MR system, with a standard quadrature head coil. The measurements were performed at the isocenter of the magnet and in a single slice. Different locations along the inner cylinder of the phantom were examined by moving it stepwise along the isocenter axis between measurements.

To evaluate the T_1 relaxation times, an Inversion Recovery-sequence (IR) was used. This sequence begins with a 180°- pulse preceding the 90°-pulse, where the time between these pulses is called the inversion time (denoted TI).
The acquired signal from an inversion-recovery sequence could in general be written as (McRobbie 2003)

$$S_{IR}(TI) = M_0\left[1 - 2e^{-\frac{TI}{T_1}} + e^{-\frac{TR-TI}{T_2}}\right]e^{-\frac{TE}{T_2}}, \qquad [1]$$

in which M_0 is the net magnetisation in a specific volume of the object, and TI the inversion time. If the repetition time is significantly longer than the inversion time, and additionally, if the T_1 relaxation time is short, approximately (TR-TI)>5T_1, eq. [1] can be simplified into

$$S_{IR}(TI) = M_0 e^{-\frac{TE}{T_2}}\left[1 - 2e^{-\frac{TI}{T_1}}\right]. \qquad [2]$$

Immediately after the 180°- pulse, T_1 relaxation takes place and the resulting magnetisation vector begins to grow in the z-direction. If the following 90°-pulse is transmitted just when the M-vector magnitude is zero in the z-direction, no echo is formed after the 90°-pulse. If the 90°-pulse is transmitted at a later time, the magnetisation vector is flipped and thus an echo is formed. If the 90°-pulse is transmitted before the magnetisation vector has become positive in the z-direction, the resulting signal has a different phase, which results in a negative signal. Hence, by varying the inversion time and evaluate the signal in the resulting images, the relaxation curve is sampled at different points and the T_1-relaxation time of the substance can be determined by fitting an appropriate function to the data points.

The inversion pulse sequence was used with TR equal to 10 s and TE equal to 14 ms. The inversion time (TI) was set to 100,200,400,800,1600 and 2400 ms. The Field-Of-View (FOV) was 192 mm square-sized, and the matrix size was 128×128 pixels. One slice was acquired with a voxel size equal to 1.5×1.5×5 mm. A region-of-interest (ROI) of approximately 350 pixels was created in the image of the inner cylinder, and the mean signal was recorded on the Siemens workstation. The calculation of the resulting T_1-relaxation times were made using a program module in IDL 6.0 (Research Systems, Inc.), where the recorded ROI values were entered and a iterative curve fit with the routine CURVE_FIT was performed, to a function of the form

$$S_{IR}(TI) = a + be^{-\frac{TI}{T_1}}, \qquad [3]$$

where S_{IR} denotes the mean signal of the ROI in the images. The equation above has the same form as eq. [2]. The curve fit used a gradient-expansion algorithm to conduct a non-linear least-squares fit. Along with the values of each parameter, the standard deviation of each parameter was also received from the workstation. To get a representative relaxation value for the gel, nine T_1 measurements were performed along the z direction of the phantom, and the average T_1 relaxation time for all positions in each gel was calculated respectively, along with the standard deviation, according to the equations

$$\overline{T_1} = \frac{\sum_{i=1}^{N}(T_1)_i}{N} \qquad [4]$$

$$SD_{T_1} = \sqrt{\frac{\sum_{i=1}^{N}\left((T_1)_i - \overline{T_1}\right)^2}{N-1}}. \qquad [5]$$

In the equations above, *N* represents the number of measurements in each gel respectively.

The evaluation of the gels´ T_2-relaxation times was done with a Carr-Purcell spin-echo sequence. This sequence begins with a 90°-pulse, where after the spin begins to dephase in the transversal plane. By sending in a 180°-pulse, the spins are being rephased and an echo is formed. The acquired signal from a Carr-Purcell spin-echo sequence can be written as (McRobbie 2003)

$$S_{SE}(t) = M_0\left[e^{-\frac{TE}{T_2}} e^{-\frac{\gamma^2(\Delta B)^2 D\tau^2 t}{3}}\right], \qquad [6]$$

in which γ is the gyromagnetic ratio, ΔB is the magnetic field inhomogenity, D is the diffusion coefficient, t is the time from the initial 90-pulse to a specific echo, and τ is the time between a 180-pulse to the following echo. If τ is small, the second exponential term in eq. [6] approaches unity and the expression can be simplified into

$$S_{SE}(t) = M_0 e^{-\frac{TE}{T_2}}. \qquad [7]$$

By collecting echoes different times after the excitation pulse, an exponential curve can be fitted to the resulting mean signal values from a ROI over the object, and the T_2-relaxation time can be estimated.

A multi-echo SE-sequence was used with an echo train of TE:s equal to 23,46,69,92,115,138 and 161 ms, and a TR equal to 1000 ms. One slice was aquired per excitation with a slice thickness of 5 mm. The FOV was a 220 mm square with 256×256 pixels. The T_2 evaluation of the images was done using software on the Siemens Allegra system. Images were taken along the z-direction of the phantom, and totally 15 images were acquired. To evaluate the T_2 values, circular ROI:s were placed in the calculated T_2 images at a position corresponding to the center of the inner cylinder. The ROI values resulted in a mean value of the T_2 relaxation time and a corresponding standard deviation. Finally, a mean value of the T_2 relaxation time for each gel was calculated according to eq. [4] and eq. [5].

The T_2*-relaxation times were measured using a gradient echo sequence. As opposed to the spin-echo sequence, the gradient echo sequence does not compensate for local magnetic field inhomogeneity effects. This causes a more rapid dephasing compared to the usual T_2-relaxation. The acquired signal from a gradient-echo sequence after equilibrium can be expressed as (McRobbie 2003)

$$S_{GE}(TE) = M_0 \frac{\sin\alpha\left(1 - e^{-\frac{TR}{T_1}}\right)e^{-\frac{TE}{T_2^*}}}{1 - \cos\alpha\, e^{-\frac{TR}{T_1}}} . \qquad [8]$$

If the echo time is the only dependent variable, leaving the repetition time and the flip angle constant, eq. [8] can be simplified into

$$S_{GE}(TE) = S_0 e^{-\frac{TE}{T_2^*}}, \qquad [9]$$

where T_2^* always is shorter than T_2 in human tissues. By using different echo times, the T_2^*-relaxation time could also be estimated by fitting an exponential function to the mean signal values of a ROI.

The T_2^* measurements were performed at one position in each gel of the inner cylinder. The position in each gel were two centimetres into each gel, from the borderline between the gels. These two positions were approximately similar to the slice positions used in the BOLD measurements.

The sequence parameters were TR=1000 ms, a 128×128 pixel map with a quadratic FOV equal to 192 mm, and a flip angle equal to 25°. The slice thickness was 5 mm. The echo times were identical to the ones used in the spin-echo sequence (23,46,69,92,115,138,161 and 184 ms). In each image, a ROI was placed and the mean value of the ROI was used to fit a function in an IDL program. The fitted function had a form of

$$S_{GE}(TE) = a + be^{-\frac{TE}{T_2^*}} . \qquad [10]$$

The program used for curve fitting was based on a iterative curve fit with the routine CURVE_FIT in the IDL program language. The program yielded the calculated values of the variables in eq. [10] and their standard deviations. No background correction was used during the evaluation of the T_2^* values.

2.4. Evaluation program and analysis parameters

To evaluate the data from the phantom measurements, a computer program has been written in IDL (version 6.0, Research Systems Inc.), which offers a fast overview of the results from the phantom measurements. The program offers evaluation parameters such as CNR-maps, T-test, ROI evaluations, stability measurements, Weisskoff stability test (Weisskoff, 1996), centre-of-

mass evaluations and more which is described below. A further assignment is to integrate the program as a routine in the existing framework of LUPE (the LUnd PErfusion program, MR physics Lund). A screen shot of the program is presented in figure 7 below.

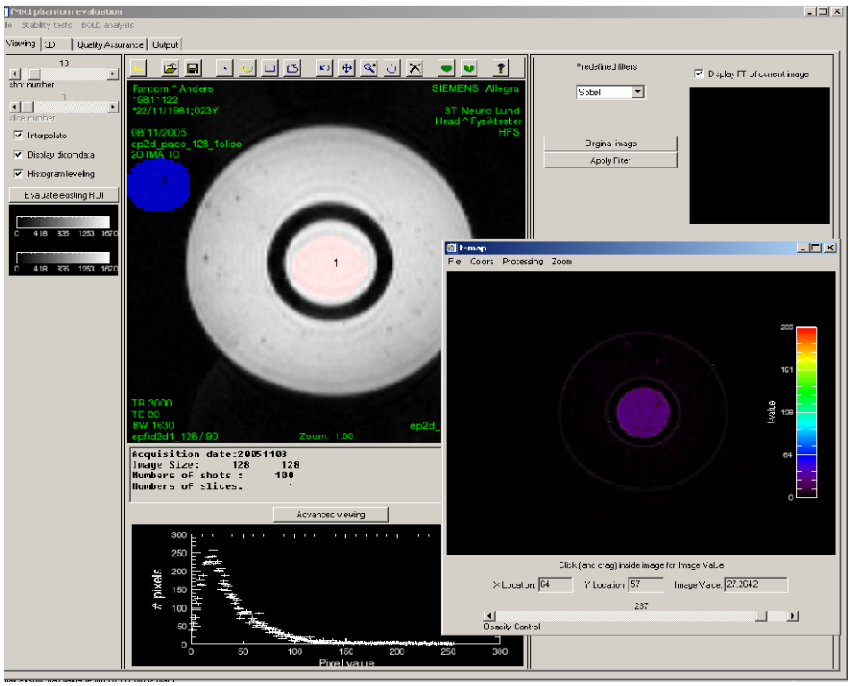

Figure 7. The QA program written in the IDL language used for image evaluation.

A useful parameter in BOLD measurements is the signal difference between an activated state and baseline state. This can be expressed as percent signal change (PSC), and can be written as

$$PSC = 100 \cdot \frac{\overline{S_{act}} - \overline{S_{rest}}}{\overline{S_{rest}}}, \qquad [11]$$

where $\overline{S_{act}}$ and $\overline{S_{rest}}$ denotes the mean signal in the images from the activated and rest state respectively, measured in a specific area. The PSC value increases linearly with the field strength, and typical PSC values are in clinical BOLD imaging a value of 1 – 5 % for a field strength of 1.5 - 3 T (Voets et al 2005), depending on the chosen echo time. For field strengths of 1.5 T, a PSC value of 1 - 2 % can be expected (Parrish et al 2000). A PSC value in the range of 1 – 5 % at an echo time of 30 ms was determined to be desirable for the phantom. The PSC can be calculated in the evaluation program as a map, presenting the PSC for each pixel in the time series.

To describe the image quality, the Signal-to-Noise ratio, denoted SNR, is often used. The SNR value is in its simplest form the ratio between the mean signal and the standard deviation of the white noise;

$$SNR = \frac{\overline{S}}{\sigma_g} \qquad [12]$$

in which $\overline{S}$ is measured as the mean signal from a ROI placed over the object in the image. The standard deviation of the noise σ_g can be measured in a ROI placed outside the object, free from possible artefacts and signals from other objects. However, due to the fact that the MR signal is complex and that most MR images are presented as magnitude images, the resulting noise do not have a zero mean, and tends to deviate from the normal distribution at low SNR-ratios (Johanssson 2000). Therefore, the standard deviation of the noise is corrected by the equation

$$\sigma_g = \frac{1}{\sqrt{\pi/2}} \cdot S_{noise}\,, \qquad [13]$$

in the above equation S_{noise} represents the mean signal value from the ROI placed outside the object. To get a better quantification of the noise, multiple ROI:s can be put outside the object, and the mean value of these multiple ROI:s be used in eq. [13].

When dealing with more images than one, an alternative way to estimate the Signal-to-Noise ratio can be useful. The SNR ratio is then determined from a mean value of a ROI covering the object in one of multiple images, and the standard deviation from the same ROI in a difference image, that is

$$SNR = \frac{\sqrt{2} \cdot S_n}{\sigma_{diff}} \qquad [14]$$

S_n is the mean value of the ROI covering the object in one of the consecutive dynamic images taken with the same imaging parameters, and σ_{diff} denotes the standard deviation from the same ROI over the difference image (Och *et al.* 1992). The factor $\sqrt{2}$ arises from the greater standard deviation of the difference image due to the subtraction (McRobbie 2003).

In terms of evaluating the stability, the evaluation program offers a number of useful stability parameters. One simple way of evaluating the stability is to make a ROI in the object in each image throughout the time series, and use the standard deviation and mean values of these ROI:s to get an estimate of the stability. In the constructed IDL program the stability is defined as

$$Stability = 100 \cdot \frac{\sqrt{\frac{\sum_{n=1}^{N}\left(S_n - \overline{S}\right)^2}{N-1}}}{\frac{1}{N}\sum_{n=1}^{N} S_n} \quad [\%]. \qquad [15]$$

The above equation can be seen as the standard deviation of the ROI:s in the time series, divided by the corresponding mean values of the ROI:s in the time series.

Weisskoff (Weisskoff R.M 1996) describes a measure of stability, which evaluates signal fluctuations as a function of ROI size. This type of stability measurement has been implemented in the IDL program, but is not currently in use.

Another measurement of stability is Centre-of-mass evaluation (denoted COM), which calculates the signal centre of mass in x- and y-direction in each image in the time series. For example, the centre-of-mass in the x-direction is calculated as

$$COM_X = \frac{1}{\sum_{x,y} S(x,y)} \sum_{x=1}^{N_X} \sum_{i=1}^{N_y} S(x, y_i) \cdot x \qquad [16]$$

Where $S(x,y)$ is the pixel value in the position (x,y) in the image.

In the statistical analysis of the BOLD series, a t-map is often calculated, presenting the t-value of each pixel in the time series. The t-value describes the probability of two sample populations having significally different means, and is calculated as

$$T = \frac{\overline{S_{act}} - \overline{S_{rest}}}{\sqrt{\frac{\sum_{i=1}^{N}\left(S_{act,i} - \overline{S_{act}}\right)^2 + \sum_{y=1}^{M}\left(S_{rest,i} - \overline{S_{rest}}\right)^2}{N+M-2}\left(\frac{1}{N} + \frac{1}{M}\right)}}, \qquad [17]$$

in which $\overline{S_{rest}}$ and $\overline{S_{act}}$ are the mean pixel value from the baseline and activated states throughout the time series, and *N* and *M* are the total number of activated and baseline states in the time series. This calculation is done (after excluding the first image in each block) with the function TM_TEST in the IDL language, and produces a t-map of the t-values for each pixel in the time series, and a corresponding significance map.

2.5. Stability measurements

The phantom was used to measure signal stability over time for clinical BOLD protocols, which is a well known quality assurance procedure in fMRI (Weisskoff 1996). The phantom was positioned at the isocenter of the MR scanner, where after the specific clinical BOLD protocols used for each camera was used. For the Siemens Allegra system, a gradient EPI sequence with TE/TR=30/3000 ms and a 64×64 matrix was used, together with a voxel size of 2.3×2.3×2.3 mm and 45 transversal slices. The same quadrature head coil used for clinical BOLD measurements on the Siemens Allegra system was used for the stability measurement. The stability was evaluated in slice 22 of the BOLD sequence, corresponding to the centre of the phantom in the z-direction.

For the stability measurement on the Philips Intera system, a TE/TR equal to 35/3000 ms was used together with a 64×64 matrix size, a slice number of 5, and the voxel size was 3×3×3 mm. A 8 channel SENSE head coil (SENSitivity Encoding) was used on the Philips system. The stability was evaluated in slice number 3.

Each measurement resulted in 300 images taken over a period of 15 minutes. No parts of the phantom were moved during the stability measurements. Stability was evaluated using the analysis software written in this work (see chapter 2.2). A ROI was placed covering the inner cylinder and most of the outer cylinder (~2000 pixels) and the stability was calculated according to eq. [15]. Furthermore it could be seen that a ROI over the entire image (~4096 pixels) instead of a circular ROI yielded little difference with respect to the stability.

2.6. BOLD measurements

The BOLD measurements were made on the Siemens Allegra Magnetom 3T system (Siemens, Erlagen, Germany), with a quadrature head coil. The camera was selected to be used for this work because of all clinical fMRI examinations in Lund at present were performed solely on this 3 T camera system.

Volume shimming (first and second order) was performed with the inner cylinder positioned at isocenter, i.e. the gel boundary was placed in the isocenter along the z-axis. This initial position of the inner phantom allowed the necessary movement of the inner cylinder to be less than two centimetres in each direction during imaging with respect to the position during shim acquisitions. The imaging parameters were TE/TR equal to 30/3000 with a quadratic 192 mm Field-Of-View, a bandwidth of 1628 Hz/pixel, a voxel volume of $1.5 \times 1.5 \times 3$ mm^3 and a 90° excitation pulse. The matrix size was 128 pixels and the number of slices was one. The paradigm consisted of totally 102 volumes, with the first two volumes automatically excluded (dummy scans). Each block (rest and active, respectively) consisted of 10 volumes. The movement of the inner cylinder was done manually using a long wooden stick attached to the lid of the inner cylinder. The slice positions during imaging were approximately 2 centimetres into each gel from the boundary between the gels. To control the position of the inner cylinder during imaging, the desired positions of the inner cylinder during activation state and non-activated state were marked with stripes on the cylinder. The positioning of the inner cylinder during imaging presents a factor of uncertainty. This uncertainty of positioning the inner cylinder is estimated to be approximately equal to ±0.5 cm at each endpoint.

During the evaluation of the BOLD series, the first image in each block was excluded due to the T_1 effect, which means that each block contained nine useful dynamic images. A standard procedure is to exclude the first 2 - 3 images in each block (Almén et al, Stöcker et al 2005). However, it could be seen in the BOLD measurements that already after the first image, the signal intensity was relatively stabile (see figure 14). Thus, only the first image in each block was excluded from the BOLD datasets.

A t-map was calculated for each measurement with the function TM_TEST in the IDL program language, corresponding to eq. [8]. A ROI (~90 pixels) was placed in the t-map (covering the main part of the inner cylinder) in order to find the average t-value. Additionally the standard deviations of the t-values in the ROI:s were calculated according to eq. [5].

2.7. Reproducibility of BOLD measurements

To use BOLD measurements with the phantom as a constancy check of an MR system at repeated occasions, the phantom and experimental procedure needs to be evaluated with respect to its reproducibility. This was done by sequentially performing a number of BOLD measurements, to verify that the PSC was stable. During this period of repeated measurements, it is assumed that the MR system is stable.

Four BOLD sequences were performed with the same clinical BOLD sequence as the rest of the BOLD measurements. Each measurement was preceded by taking out and re-positioning the phantom in the MR scanner, which forced the scanner to acquire a new shim map for each measurement.

To further evaluate the reproducibility of the experimental procedure, BOLD measurements were done after the phantom had been turned and positioned with the front side pointing backwards (rotated 180 degrees). By doing this, some information is obtained about the possible effects of varying the geometry. To be able to quantify how the positioning affected the T_2^* relaxation times in the gels, gradient echo sequences with different echo times were executed with the phantom both in the original position and rotated. The T_2^* values were evaluated in the slice positions corresponding to the slice positions in the BOLD measurements, that is approximately two centimetres into each gel from the boundary between the gels.

2.8. TE optimisation

An important expression in BOLD imaging is the Contrast-to-Noise Ratio, denoted CNR. This quantity is defined as

$$CNR = \frac{\overline{S_{act}} - \overline{S_{rest}}}{\sigma_{rest}}, \qquad [18]$$

where $\overline{S_{rest}}$ and $\overline{S_{act}}$ denotes the mean signal intensities from a specific voxel in the imaging volume, corresponding to the two states that are compared. σ_{rest} represents the noise, calculated as the standard deviation of the baseline signal.

The signal arising from the BOLD response is dependent on the T_2*-relaxation time of the tissue. As discussed in the introduction section, the BOLD response gives a signal difference between activated and non-activated GBM, where the signal of the baseline state can be expressed as (Posse et al 1999):

$$S_{TE}(TE) = S_0 e^{-\frac{TE}{T_2^*}} + g + h \qquad [19]$$

in which g and h represents the white noise (the noise from thermal noise and hardware instabilities) and physiological noise, respectively), and S_0 the initial signal strength. The physiological noise can not be measured with the present phantom, and hence this term is neglected. If the difference in T_2* between activated and non-activated tissue is expressed as ΔT_2 * , the signal difference between activated state and baseline state could be written as (Posse et al 1999):

$$\Delta S(TE) = S_0 e^{-\frac{TE}{T_2^*}} - S_0 e^{-\frac{TE}{T_2^* + \Delta T_2^*}} \qquad [20]$$

and by expanding the relaxation time difference ΔT_2 *, provided that the relaxation time difference is small, the signal difference can be written as

$$\Delta S(TE) \approx S_0 \Delta T_2^* \frac{d}{dT_2^*} e^{-\frac{TE}{T_2^*}} = S_0 \frac{TE \Delta T_2^*}{(T_2^*)^2} e^{-\frac{TE}{T_2^*}} \qquad [21]$$

This expression is illustrated in the figure below.

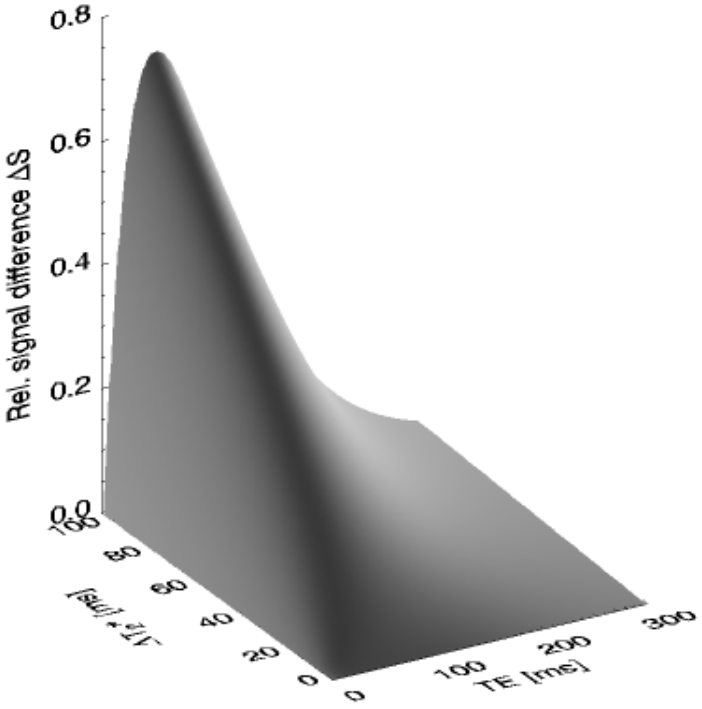

Figure 8. The BOLD signal difference depending on the echo time and the difference in T_2.*

To optimise the BOLD contrast, the maxima of eq. [21] have to be found. This is found by differentiating eq. [21] with respect to the echo time;

$$\frac{d(\Delta S)}{d(TE)} = \frac{S_0 \Delta T_2 *}{(T_2 *)^2} e^{-\frac{TE}{T_2 *}} \left[1 - \left(\frac{TE}{T_2 *} \right)^2 \right] \qquad [22]$$

where the maxima is found when the echo time equals the T_2* for the baseline state, i.e. $TE = T_2 *$.

The relationship between the signal difference ΔS and the corresponding t-value is (Parrish *et al* 2000):

$$t = \frac{\Delta S \sqrt{N}}{2\sigma_{rest}} \qquad [23]$$

in the expression above N represents the total numbers of acquired images, and σ_{rest} denotes the standard deviation of the noise, corresponding to the standard deviation of the baseline signal. Eq. [23] is similar to eq. [17], assuming that the baseline images and activated images have similar standard deviations. By eq. [23] and eq. [21] an expression for the t-value dependence of TE becomes

$$t(TE) = \frac{\sqrt{N} S_0 TE \Delta T_2^*}{\sigma_{rest} (T_2^*)^2} e^{-\frac{TE}{T_2^*}} \quad [24]$$

thus, the t-value is dependent on echo time. By using eq. [18] and eq. [21], the CNR is shown to also be dependent of the echo time:

$$CNR(TE) = \frac{S_0 TE \Delta T_2^*}{\sigma_{rest} (T_2^*)^2} e^{-\frac{TE}{T_2^*}} \quad [25]$$

by differentiating Eq. [24] and Eq. [25] with respect to the echo time, it is seen that both the t-value and CNR should have maximum values when $TE = T_2^*$, similar to the PSC.

To verify the use of the phantom to find the optimum value of an image parameter, the optimal echo time was evaluated on the Siemens Magnetom Allegra 3T using a number of BOLD sequences with echo times equal to 10,20,30,40,50,60,80 and 100 ms. The BOLD sequence was identical to the sequence used in the BOLD measurements, except for the matrix size (64·64 pixels) and the bandwidth (3004 Hz/pixel). The bandwidth was changed to allow the echo time to be low.

The signal difference was calculated by using a ROI (~90 pixels) placed in each image, covering the inner cylinder. After excluding the first image in each block, the ROI values from each image were sorted as activated and baseline images, where after the mean value of these ROI values were calculated, respectively for the activated and baseline state. The signal difference was calculated as the difference between these two mean values. Finally, the standard deviation for this signal difference was calculated by using error propagation.

The t-values were calculated as described in chapter 2.6.

3. Results

3.1. Phantom properties

The results of the T_2-relaxation time measurements made on the Siemens Allegra camera system for the inner phantom is presented in figure 9 below. 15 slices were evaluated, with the first four slices closest to the centre separated by a distance of one centimetre and the other slices by two centimetres.

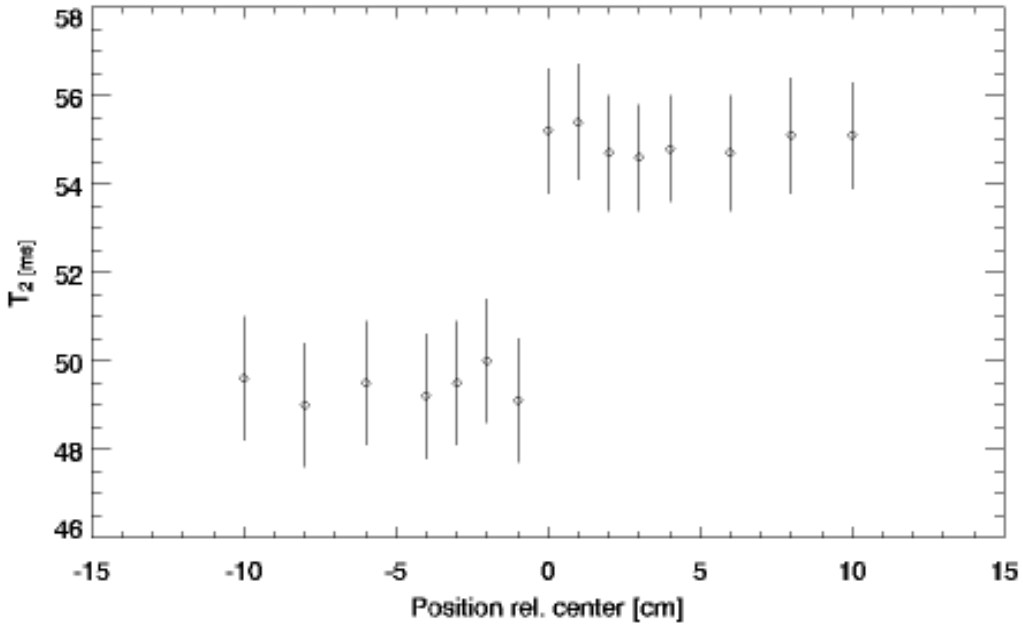

Figure 9. Measured T_2 values in the inner cylinder depending on position relative cylinder center (cylinder axis). Error bars show standard deviations. Measurements performed on the Siemens Allegra camera system.

The results shows that the average T_2 relaxation time in the gel representing activated state is 54.9±0.5 ms (average ± 1 SD, n=7), and in the gel representing baseline state 49.4±0.5 ms (average ± 1 SD, n=7).

The results of the T_1 evaluation, corresponding to nine images positioned symmetrically and equidistantly along the phantom, are shown in figure 10. The data points indicate a small variation in T_1 relaxation times along the inner cylinder, ranging from 1260 to 1320 ms. More information is available in Appendix 1.

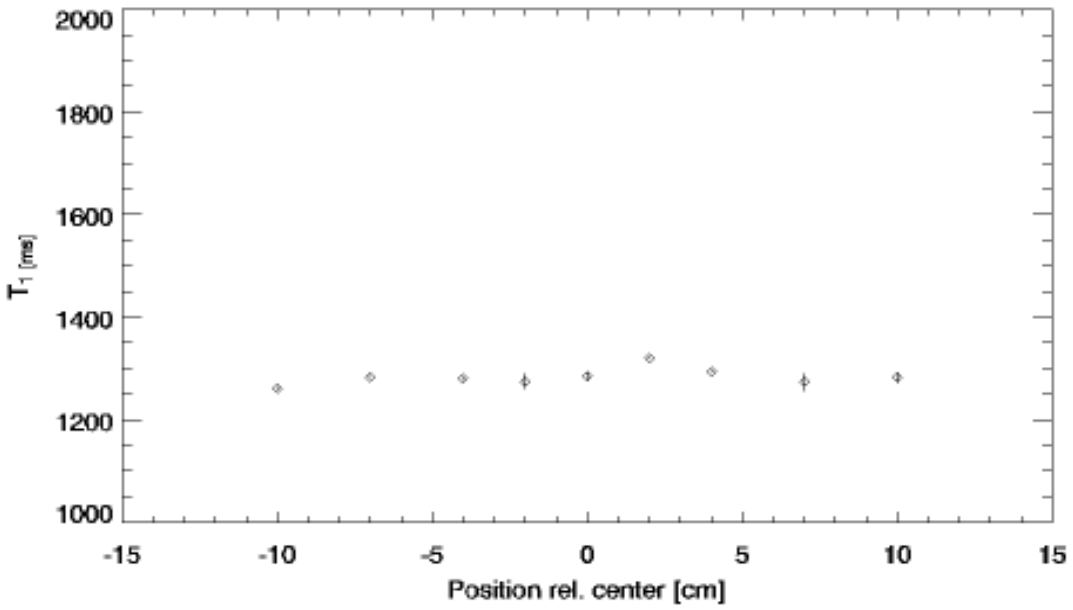

Figure 10. Measured T_1 relaxation values in the inner cylinder depending on the position along the cylinder length relative to the centre. Error bars show standard deviations obtained from curve fitting. Measurements performed on the Siemens Allegra 3T camera system.

The average T_1 relaxation time in the activated gel was found to be 1293±5 ms (average±1 SD, n=4) and 1275±4 ms (average±1 SD, n=4) in the gel representing baseline state.

The T_2* relaxation time was measured in the two positions at which the inner cylinder was imaged during the BOLD measurements. Thus, the T_2* relaxation time was measured approximately two centimetres into both gels, from the centre. In the gel representing the activated state, the T_2* was found to be 47.8±0.6 ms. In the gel representing the baseline state it was found to be 41.4±0.9 ms.
Both values are approximately 8 ms shorter compared to the T_2 relaxation times, indicating some influence of magnetic field inhomogeneities.

3.2. Stability measurements

The stability measurements from the Siemens Magnetom Allegra 3T system and the Philips Intera 3T system are presented in figures 11 and 12 below. The stability measurements revealed a stablility equal to 0.14 % in slice number 22 for the Siemens Magnetom Allegra 3T system, and a stability equal to 0.16 % in slice 3 on the Philips Intera 3T system.
No significant differences were found between the two camera systems with respect to their stability.

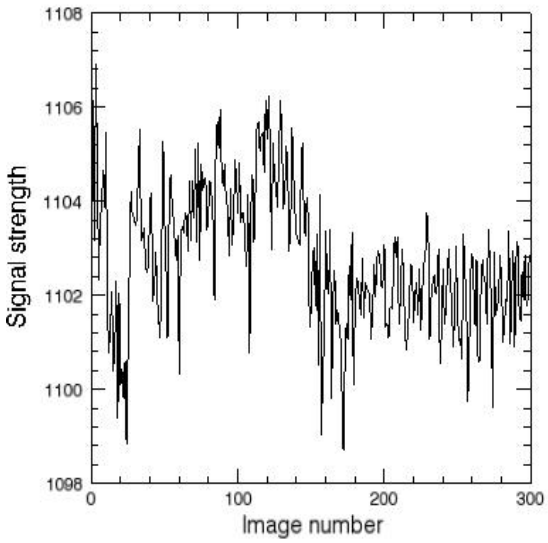

Figure 11. Stability measurement on the Siemens Magnetom Allegra 3T system, slice 22 (ROI=2011 pixels).

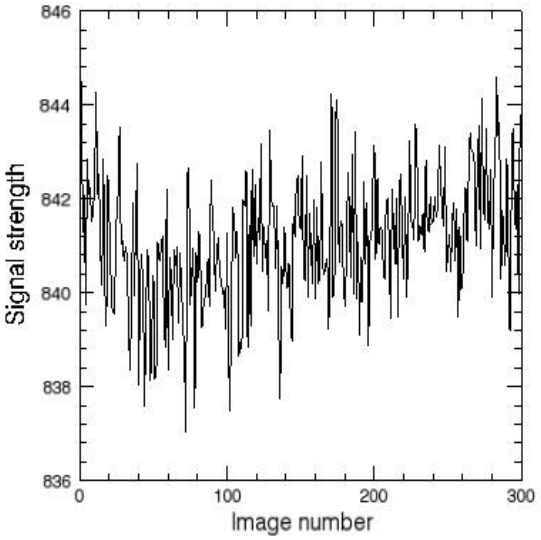

Figure 12. Stability measurement on the Philips Intera 3T system, slice 3 (ROI=1208 pixels).

3.3. Reproducibility of BOLD measurements

During the first experiments, no wooden stick was used to move the inner cylinder during imaging; instead the cylinder was moved/pushed by hand. From these experiments, it was found that the presence of the hand affected the results. To be certain, an experiment was performed in such way that during a BOLD sequence of 20 images, eight images was taken with the phantom in the same position, where after a hand was held about two centimetres in front of the phantom. The phantom did not move during the sequence. A ROI was placed in the phantom images and the mean signal value in each ROI was plotted. The results indicate a signal drop after the hand was placed in front of the phantom. The result is seen below in figure 13.

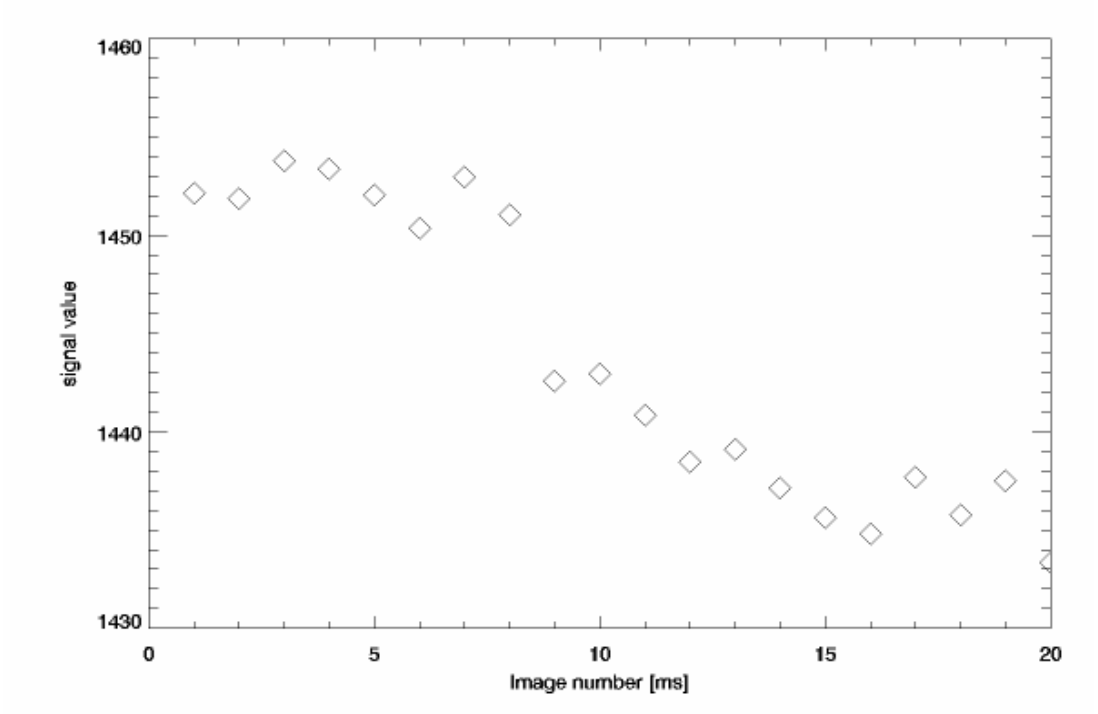

Figure 13. Mean ROI signal values from images in a BOLD sequence, acquired on the Siemens Allegra camera system. The hand was placed in front of the phantom after image number eight, and held at constant position during the rest of the measurements.

To exclude this effect of the hand, a wooden stick was used to move the inner cylinder in all BOLD examinations in this work.

An example of typical signal values for a pixel located in the centre of the inner cylinder during a BOLD sequence is presented in figure 14 below. The signal peaks in the beginning of each block arises from a T_1 relaxation effect and the first image in each block are therefore excluded. As a notice, the minor peak seen in the end of each activated-block is originating from the T_1 effect in the first image in each rest-block, as expected. Thus these minor peaks do not belong to the images in the activated block.

A typical t-map resulting from a similar BOLD sequence is presented in figure 15.

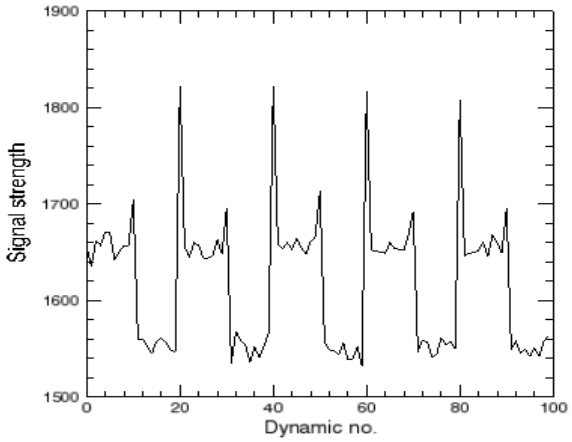

Figure 14. A typical time series from a single pixel located at the centre of the inner cylinder during a BOLD sequence, acquired on the Siemens Allegra camera system.

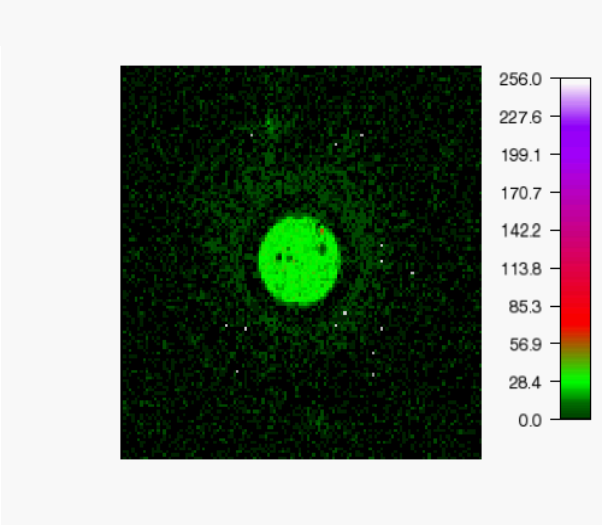

Figure 15. A typical t-map from a BOLD sequence of 100 images in ten blocks. Every first image in each block was excluded. Measurements performed on the Siemens Allegra camera system.

The four BOLD measurements performed to evaluate the reproducibility resulted in a PSC equal to 7.0±0.3 % , 6.9±0.2 %, 7.0±0.2 %, and 7.0±0.3 %.

The BOLD sequence with the phantom facing backwards yielded a PSC equal to 8.7±0.6 %. An identical BOLD sequence directly after the first measurement, with the phantom positioned forwards (correct position) yielded a PSC equal to 7.2±0.6 %. This indicates that the experimental geometry can influence the results of the BOLD measurements.

3.4. TE optimisation

The results from the BOLD measurements with varying echo times are presented below in figure 16.

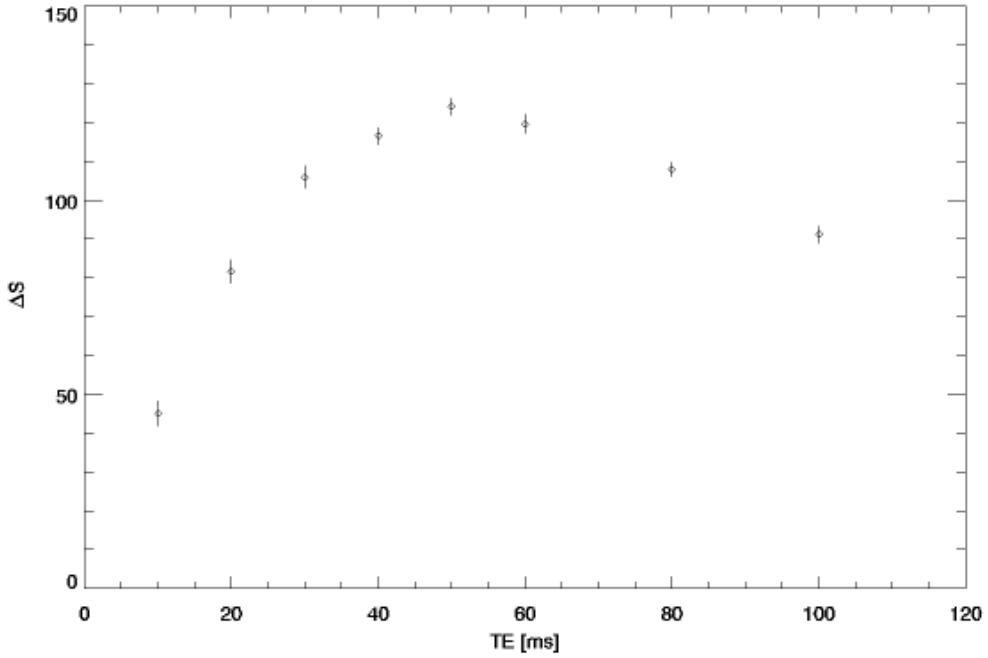

Figure 16. Signal differences between activated and baseline state in BOLD series depending on echo time. Error bars show standard deviations.

The difference in signal shows a maximum when the echo time is approximately 50 ms. This deviates somewhat from the theoretically expected maximum, which should be close to the baseline T_2^* (41.4±0.9 ms).
The t-value dependence on the echo time is presented in figure 17 below. The maximum t-value was acquired at TE~50 ms.

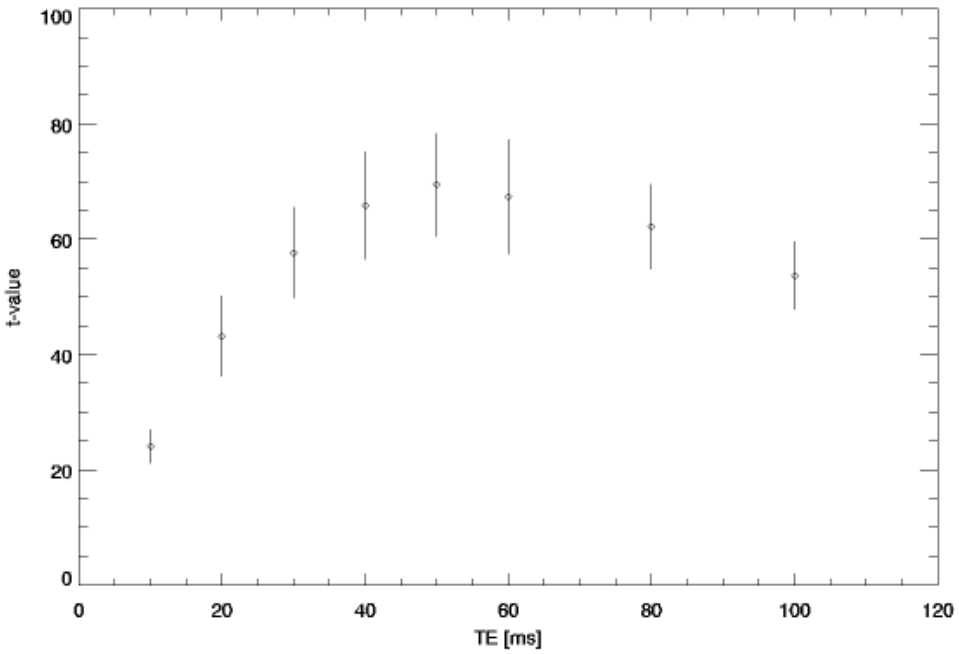

Figure 17. Calculated t-values from BOLD sequences depending on echo time. Error bars show standard deviations.

4. Discussion

The relaxation properties of the phantom were found to be close to the theoretically desired values; this indicates that manufacturing a gel with desired relaxation times is feasible. The deviation from the desired T_2 relaxation values depends primary on the accuracy of the weighting of the chemicals; if scales with better accuracy could be used, even smaller deviations would possibly be achievable.

Both gels in the inner cylinder were found to have uniform relaxation values over the chamber lengths.

A comparison of the T_2 and T_2^* relaxation values of the gels in the inner cylinder indicates a difference approximately equal to 10 ms; thus inhomogenity effects influence the relaxation times.

The reproducibility of BOLD measurements with the phantom was found to be good with a PSC equal to 7 %. The four BOLD series were all inside each others error limits. However, by rotating the phantom the PSC was changed significantly (8.7±0.6 %). This reveals that the phantom geometry influence the measurement, although the phantom geometry is fairly symmetrical. This might influence the result when different scanner systems are compared; hence the positioning of the phantom must be consistent.

During the BOLD measurement, the inner cylinder was initially moved back and forth with help of an assistant standing in front of the camera, moving the cylinder with the hand. The hand in the magnetic fields was found to cause signal voids, and to avoid this, a wooden stick was used. The most appropriate solution would be to have an automatic device to position the inner cylinder during imaging.

The echo time optimisation could successfully be performed with the phantom. The results support the idea to use the phantom for optimisation also of other parameters such as coil types, SENSE-factor and other scanner parameters. The deviation of the optimal echo time with respect to CNR from the measured T_2^* time of the baseline gel can possibly be explained by the assumption made in eq. [21], which assumes $\Delta T_2^* << T_2^*$, which is doubtful. Another factor is the uncertainty of the relaxation measurements of both T_2^* and T_2. Additionally, the motion of the phantom during the BOLD acquisitions could possibly present a change in the local field inhomogeneity, which could affect the result. This needs to be further investigated.

The stability measurements were done on two MR systems (Siemens Magnetom Allegra 3 T and Philips Intera 3 T), and both stability measurements revealed a stability lower than 0.2 %. No problems were encountered when using the phantom for stability measurements. No significant differences between the two camera systems were found; however, the stability measurements were too few and too short to find possible significant differences.

The good long-term stability of agarose reported by Christofferson (Christofferson *et al.* 1991) render the phantom useful for stability measurements and other QA applications over longer time.

5. Conclusions

With these results, it appears suitable to use an agarose phantom to both simulate BOLD response in order to study and optimise signal parameters such as echo time and SENSE-factor, and to perform stability tests. However, to have a sufficient reproducibility, one has to pay attention to the positioning of the inner cylinder during the shimming procedure.

The translational movement of the inner cylinder during imaging is most suitably done by automatic device, with a fixed position not to influence the magnetic field. A simple solution is to use a wooden stick to move the cylinder. No hands should be used, because of the signal voids created by the disturbance of the B_0-field.

The phantom is also well suited for stability tests.

6. Further work

Further investigation of the effects of different shim sequences would be useful to possibly minimise the inhomogenity effects and thereby keeping the T_2^* closer to T_2.

A desirable function would be to develop an automatic device to move the phantom during imaging.

Additionally, the use of the phantom in a multi-centre study is needed, in order to investigate whether the phantom can be used for comparing different systems.

7. Appendix 1: Detailed results

Table 1. Measured signal intensities for an inversion recovery sequence in inner cylinder depending on inversion time and position in phantom with standard deviations. T_1 shows the resulting T_1 relaxation times and standard deviations obtained by curve fitting signal values from each position

	Position [cm]								
TE [ms]	-10	-7	-4	-2	0	2	4	7	10
100	-1693±31	-1637±31	-1620±32	-1600±33	-1639±33	-1689±32	-1699±32	-1700±32	-1671±34
200	-1396±25	-1330±27	-1316±30	-1335±29	-1352±29	-1404±27	-1410±27	-1395±28	-1378±29
400	-872±16	-841±17	-830±18	-835±17	-859±22	-902±18	-892±18	-887±17	-874±18
800	-45±4	-42±4	-39±4	-37±4	-63±12	-92±4	-85±4	-82±4	-86±4
1600	1003±19	975±18	959±18	955±18	949±19	943±17	945±18	938±18	929±19
2800	1725±32	1689±31	1670±32	1651±32	1654±31	1689±31	1683±32	1663±33	1641±34
T_1 [ms]	1260±2	1284±2	1281±2	1275±14	1285±7	1321±1	1294±1	1274±16	1282±11

Table 2. Calculated T_2 relaxation times in different positions in the inner cylinder

Position [cm]	T_2 [ms]
0	55.2±1.4
1	55.4±1.3
2	54.7±1.3
3	54.6±1.2
4	54.8±1.2
6	54.7±1.3
8	55.1±1.3
10	55.1±1.2
-1	49.1±1.4
-2	50.0±1.4
-3	49.5±1.4
-4	49.2±1.4
-6	49.5±1.4
-8	49.0±1.4
-10	49.6±1.4

Table 3. Measured signal intensities depending on echo time for the gradient sequence used to evaluate T_2 with corresponding standard deviation, and the resulting T_2* value with standard deviations*

	Signal intensity	
TE [ms]	Activated gel	Baseline gel
23	866±17	802±21
46	542±14	472±15
69	334±9.6	265±10
92	203±7.3	149±7.9
115	124±5.9	84±6.7
138	77±5.4	46±5.6
161	47±5.5	25±5.1
184	28±5.4	14±4.9
T_2*	47.8±0.6	41.4±0.9

Table 4. Summary of measured relaxation times for the two gel types with corresponding standard deviations.

Relaxation	Active	Rest
T_1 (n=4) [ms]	1293±5	1275±4
T_2 (n=7) [ms]	54.9±0.48	49.4±0.53
T_2* [ms]	47.8±0.6	41.4±0.9

Table 5. PSC for the BOLD sequences with phantom positioned normal and backwards

Meas. no.	PSC (Forth)	PSC (Back)
1	0.070±0.003	-
2	0.069±0.002	-
3	0.069±0.002	-
4	0.070±0.003	-
5[1]	0.072±0.006	0.087±0.006

Table 6. T_2- and T_2 relaxation values in the inner chamber depending on the positioning of the phantom*

	Back		Forth	
Relaxation time [ms]	Activated	Baseline	Activated	Baseline
T_2 [ms]	-	-	54.9±0.5	49.4±0.5
T_2* [ms]	45.5±0.8	41.6±0.7	47.8±0.6	41.4±0.9

1 Measurements made three days before other BOLD measurements in table 4

Table 7. Measured signal differences in BOLD sequences depending on TE

TE [ms]	ΔS
10	45.0±3.2
20	81.6±3.0
30	105.9±2.9
40	116.6±2.1
50	124.1±2.1
60	119.7±2.4
80	107.9±1.7
100	91.2±2.2

8. References

8.1. Articles

Almén A, Ceberg C, Eberhardt J, Schallenberg B, Wirestam R, Internal report, Lund University, *Bildgivande MR-teknik - signalekvationer*

Belliveau JW (1991), Kennedy DN, McKinstry RC, Buchbinder BR, Weisskoff RM,Cohen MS,Vevea JM, Brady TJ, Rosen BR , *Functional Mapping of the Human Visual Cortex by Magnetic Resonance Imaging*, Science, 1991;254:716-719

Caparelli EC (2004), Tomasi D, Ernst T, *The effect of small rotations on R_2* measured with echo planar imaging*, Neuroimage, 2004;24:1164 - 1169

Cheng Hu (2004), Zhao Q, Spencer D, Duensing G R, Edelstein W A, *A fMRI Study of the SMARTPHANTOM*, Proc. Intl. Soc. Mag. Reson. Med. 2004;11:1041

Christoffersson JO (1991), Olsson LE, Sjöberg S, *Nickel-doped agarose gel phantoms in MR imaging*, Acta Radiologica 1991;32:426-431

Fox PT (1988), Raiche ME, Mintun MA, Dence C, *Nonoxidative Glucose Consumption during Focal Physiologic Neural Activity,* Science 1988;241:462 – 464

Friedman L (2005), Zhao Q, Cheng H, Duensing R, Greve DN, Glover GH, *Multi-center fMRI Calibration with SMARTPHANTOM*, Proc. Intl. Soc. Mag. Reson. Med. 2005;13:1529

Gore, J (2003), *Principles and practice of functional MRI of the human brain*, J. Clin. Invest. 2003;112: 4 - 9

Johansson E (2000), Laboration tutorial "MR", Lund University Hospital

Krüger G, Kastrup A, Glover G, *Neuroimaging at 1.5 T and 3.0 T: Comparison of Oxygenation-Sensitive Magnetic Resonance Imaging*, Magn. Res. Med. 2001;45:595 - 604

Kwong KK, (1992), Belliveau JW, Chesler DA, Goldberg IE, Weisskoff RM, Poncelet BP, Kennedy DN, Hoppel BE, Cohen MS, Turner R, Cheng H-M, Brady TJ, Rosen BR, *Dynamic magnetic resonance imaging of human brain activity during primary sensory stimulation*, Proceedings of the National Academy of Sciences of the United States of America, 1992;89:5675-5679

Lu H (2005), Nagae-Poetscher L, Golay X, Lin D, Pomper M, van Zijl P, *Routine Clinical Brain MRI Sequences for Use at 3.0 Tesla,* J. Magn. Res. Imag. 2005;22:13-22

Noll DC (2004), *Technical challenges in functional neuroimaging*, Department of Biomedical Engineering, University of Michigan, 2004

Och J G (1992), Clarke G D, Wladyslaw T S, Rosen C W, Mun S K, *Acceptance testing of magnetic reesonance imaging systems: Report of AAPM Nuclear Magnetic Resonance Task Group No 6*, Med. Phys. 1992 ;19:217 - 229

Ogawa S (1990), Lee T-M, Nayak A S, Glynn P, *Oxygenation-Sensitive Contrast in Magnetic Resonance Image of Rodent Brain at High Magnetic Fields*, Magn. Reson. Med. 1990;14:68 - 78

Ogawa S (1990b), Lee T M, Kay A R, Tank D W, *Brain magnetic resonance imaging with contrast dependent on blood oxygenation*, Proc. Natl. Acad. Sci. USA 1990;87:9868 - 9872

Olsrud J (2005), Waites A, Mannfolk P, *A phantom for simulation of BOLD response*, Proc. ESMRMB 2005

Parrish T B (2000), Gitelman D R, LaBar K S, Mesulam M M, *Impact of Signal-to-Noise on Functional MRI*, Magn.Reson. Med. 2000;44:925-932

Pfeuffer J (2003), McCullough J C, Van de Moortele P-F, Ugurbil K, Hu X, *Spatial dependence of the nonlinear BOLD response at short stimulus duration*, Neuroimage 2003;18:990-1000

Posse S (1999), Wiese S, Gembris D, Mathiak K, Kessler C, Grosse-Ruyken M-L, Elghahwagi B, Richards T, Dager S R, Kiselev V G, *Enhancement of BOLD-Contrast Sensitivity by Single-Shot Multi-Echo Functional MR Imaging,* Magn. Reson. Med. 1999;42:87 - 89

Svensson J, Universitetssjukhuset MAS (Information by personal communication)

Stöcker T (2005), Schneider F, Klein M, Habel U, Kellerman T, Zilles K, Shah N J, *Automated Quality Assurance Routines for fMRI Data Applied to a Multicenter Study*, Human Brain Mapping 2005;25:237 - 246

Van Westen D (2005), Skagerberg G, Olsrud J, Fransson P, Larsson E-M, *Functional Magnetic Resonance imaging at 3T as a Clinical Tool in Patients with Intracranial Tumors,* Acta Radiologica 2005;46:599 - 609

Voets N L (2005), Matthews, P M, *Clinical Applications of Functional Magnetic Resonance Imaging*, Imaging Decisions MRI, Blackwell Publishing 2005;9:16-22

Weisskoff, R M, (1996), *Simple Measurement of Scanner Stability for Functional NMR Imaging of Activation in the Brain*, Magn. Reson. Med. 1996;36:643 - 645

8.2. Internet sources

Lorberbaum, J P, *Functional Magnetic Resonance Imaging (fMRI) for the Psychiatrist*, http://www.musc.edu/psychiatry/fnrd/primer_fmri.htm , 050506

8.3. Books

McRobbie, D.W et al, *MRI From Picture to Proton*, Cambrigde University Press, 2003, ISBN 0-521-52319-2

9. Acknowledgements

First of all, thanks to my supervisor Johan Olsrud for helping me, giving me advice and excellent guidance. The other physicists at the MR department, Peter Mannfolk, Antony Waites and Karin Markenroth, have also contributed greatly by giving me good laughs, help and ideas. And at last, thanks to all members in the MR physics group and the personnel at the MR department at the Lund University Hospital, for the kindness of letting me stay there during my work.